

USING SMALL-APERTURE ARRAYS TO IDENTIFY FAR-REGIONAL P-WAVE ARRIVALS

Aaron Ferris¹ and Delaine Reiter¹

Weston Geophysical Corp.¹

Sponsored by Air Force Research Laboratory

Contract No. FA8718-06-C-0002

ABSTRACT

Seismic observations recorded at far-regional distances contain information that could potentially be highly useful to monitoring seismologists. However, that information is currently under-utilized, because of propagation complexities that cause significant difficulties in the interpretation of seismograms. At far-regional distances ($\sim 14^\circ$ – 18°) seismic waves sample upper-mantle heterogeneities and the discontinuities at approximately 410 and 660 km depth, and this interaction results in triplications and interference phenomena in the observed data. In central Asia, these complications along the propagation path produce travel-time bulletins that exhibit large residuals (1–8 s) for the direct *P* arrival from far-regional events.

The regional seismic arrays that have been built in the last fifteen years should be rich sources of data for the study of far-regional wave phenomena. Unfortunately, the aperture of many modern regional arrays is so small (~ 2 – 3 km) that any study of phase characteristics beyond accurate picks of primary phase onset times is quite difficult. The goal of our project is to develop methods that can increase the accuracy of primary and early coda phase identification at currently deployed small-aperture regional arrays. These methods include modifications to two well-known τ -p filtering (or velocity spectra analysis) methods: Nth-root and phase-weighted stacking. We have applied our methods to vertical-component data recorded at distances between 14° – 18° by small-aperture arrays in central Asia. Our results indicate that in many cases we can identify closely spaced arrivals by their slowness values in a time window that includes the direct *P* arrival, depth phases and arrivals from upper-mantle discontinuities.

OBJECTIVE

The major upper-mantle discontinuities at approximately 410- and 660-km depth have a strong effect on the patterns of body-wave arrivals observed between epicentral distances of 15° – 27° . At far-regional distances (14° – 18°), there are typically several P arrivals occurring within the first 15–25 s of the seismogram, with horizontal slowness values ranging from 8–11 s/deg. In a 1-D reference model such as IASPEI91 (Kennett and Engdahl, 1991), these arrivals include the direct P arrival, a refracted arrival from 165 km depth, and refracted arrivals from the 410-km and 660-km discontinuities. The triplications from the main P phases are also complicated by possible depth phases, which have equivalent travel-time curves at a positive time offset that depends on earthquake depth and the velocity structure above the source. The seismograms may be further complicated by upper-mantle heterogeneities encountered along the source-to-receiver path.

For example, in central Asia the travel-time bulletins of far-regional events exhibit large travel-time residuals (1–8 s) for the direct P arrival. These residuals are likely due to a combination of phase identification errors and inadequate upper-mantle models in the region. The goal of our research is to improve phase characterization in the early body-wave coda observed at far-regional distances. An important component of our research is the development and application of accurate array-processing techniques to the triplicated arrivals observed at small-aperture arrays installed in central Asia.

RESEARCH ACCOMPLISHED

To address our research objective we are using array-based methods that can differentiate between closely spaced arrivals in array seismograms. Numerous array-processing techniques have been developed to lower the detection threshold for small events by suppressing noise and enhancing coherent signal. Techniques such as frequency-wavenumber (f - k) or travel-time slowness (τ - p) analysis are commonly used for array-based signal characterization. In the case of f - k analysis, the apparent slowness and back azimuth of a signal can be determined from the 2-D Fourier transform of an array signal. In τ - p processing, the array seismograms are mapped into travel-time slowness (or back-azimuth) space by employing slant-stack summation or Velocity-Spectra Analysis (known as *vespa* processing). Both of these methods can be successfully used to identify a secondary arrival via its slowness value.

However, the small aperture (\sim 2–3 km) of many of the newer arrays installed for nuclear monitoring purposes presents a serious problem for f - k and τ - p methods at far-regional distances. For an array slant stack to resolve the slowness of secondary arrivals, array elements must have an inter-element spacing that produces time shifts of at least several samples over a reasonable range of slowness values. Figure 1 illustrates this effect using synthetic seismograms and two six-element arrays of 3- and 25-km apertures. We modeled the response of the arrays for a 5-km deep event at 16° epicentral distance using a reflectivity method and the AK135 reference model (Kennett et al., 1995), adding Gaussian noise at a 3 dB level to the resulting waveforms. Then we calculated a 4th-root slant stack of the synthetics over the initial wavetrain for a slowness range from 0.5–0.25 s/km. The red circles in the vespagrams (bottom panels) of Figure 1 mark the slowness-time peaks averaged for regions containing energy within 15% of the maximum; the circles' diameters illustrate the standard errors in the peak measurement.

Phase arrivals from this distance take \sim 0.2 s to cross the 3-km aperture array and \sim 2.5 seconds to cross the 25-km aperture array. For the closely spaced elements of the 3-km aperture array, small slowness values (high horizontal phase velocity) result in time shifts of only a few samples (1–6) between array elements, producing poorly resolved apparent arrival slowness. This is clearly apparent in the comparison between the bottom subpanels in Figure 1, in which the vespagram of the 3-km aperture array is heavily smeared along the slowness axis compared to the vespagram of the 25-km aperture array.

This smearing effect in slowness space for small-aperture arrays is the primary obstacle to the development of robust array-processing techniques at far-regional and near-teleseismic distances. To address the problem we have adapted some familiar processing techniques, such as the N th-root and phase-weighted stacking, to our specific problem.

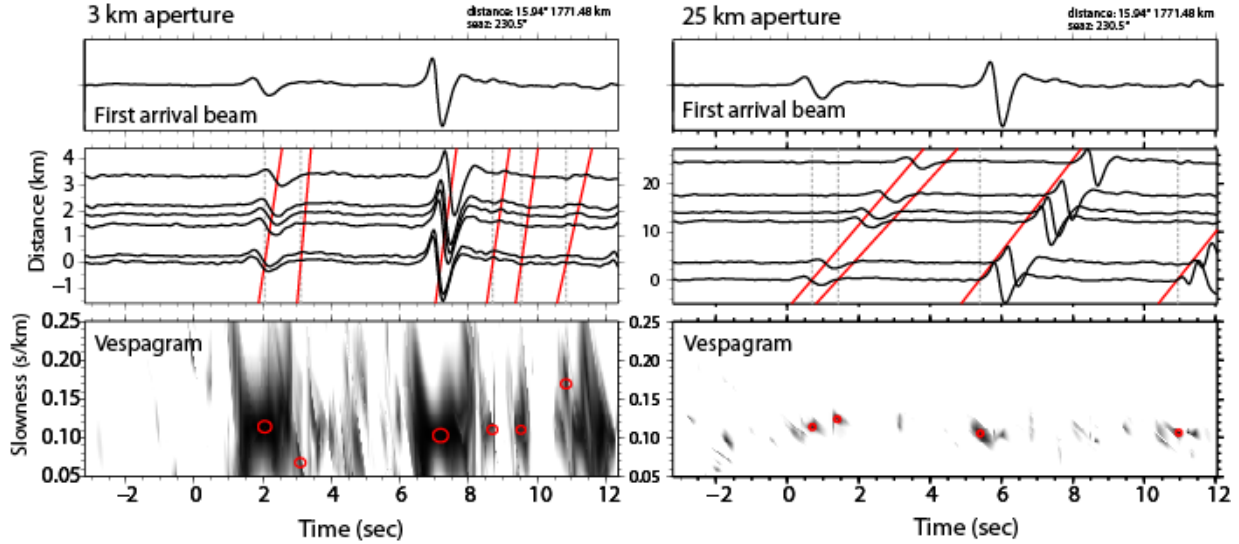


Figure 1. A synthetic example of the slant-stack process for a far-regional event recorded at a 3-km aperture array (left) and a 25-km aperture array (right). Top panels show the array beam computed using the first-arrival slowness value. Middle panels show the array elements sorted by distance. Red lines show the travel-time curves for the slowness values determined from the 4th-root vespagrams (bottom panels). The slowness vespagrams for both arrays are plotted at the same color scale, and red circles mark the time-slowness peaks, averaged for vespa regions containing energy within 15% of the maximum.

Array Processing Methods for Small-Aperture Regional Arrays

We analyze the early P -wave coda of far-regional observations on small-aperture arrays using two τ - p processing methods that are commonly used in phase identification (for a general survey of techniques, see Rost and Thomas, 2002). The first method is known as N th-root stacking (Muirhead and Datt, 1976) and the second as phase-weighted stacking (Schimmel and Paulssen, 1997). Both techniques are variations on the slant-stack method, in which waveforms are beamed for a range of slowness values and a known back azimuth. The beam power is then displayed as a function of travel time and slowness; these images are commonly referred to as vespagrams or vespas (Velocity Spectral Analysis). The two vespa techniques differ in the mechanism employed to enhance weak arrivals and suppress incoherent signal, as we explain below.

*N*th-root stacking analysis

To form an N th-root stack, the signed N th-root (N) of each array trace (s_j) is taken before beam summation over the M array traces, for a given slowness value (u) and time sample (t), i.e.,

$$v'_{u,N} = \frac{1}{M} \sum_{j=1}^M |s_j(t - t_{u,j})|^{1/N} \frac{s_j(t)}{|s_j(t)|}. \quad (1)$$

After summation across the array, the beam is raised to the N th-power and the saved sign is applied:

$$v_{u,N} = |v'_{u,N}|^N \frac{v'_{u,N}}{|v'_{u,N}|}. \quad (2)$$

Increasing the value of N decreases the amplitude variation in a trace; this boosts the amplitudes of coherent, small amplitude arrivals and decreases the dominance of large amplitude arrivals. In our application at small-aperture arrays it is necessary to accentuate very small differences in potential slowness maxima across the smeared slowness

axis. Therefore, we have selected a root value of $N = 15$ to enhance coherent arrivals and allow us to more easily pick a slowness peak in the N th-root vespagram. Figure 2 illustrates how smaller values of N produce broader peaks in the vespa image, making slowness determination less precise. In addition, to further enhance coherent, small-amplitude arrivals, we perform the 15th-root stacking in sliding window segments of 1.5 to 3.0 s along the entire signal window of interest.

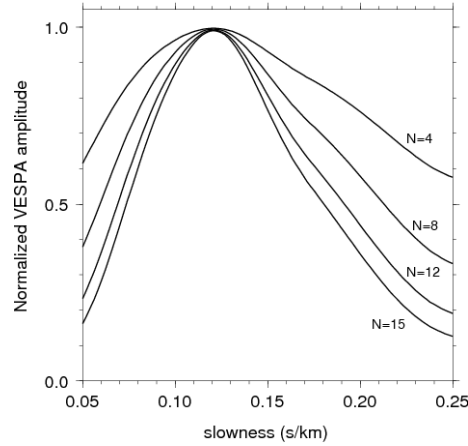


Figure 2. Time slice ($t = 2.0$ s) through the 3-km aperture vespagram shown on the left in Figure 1 for increasing values of the N th root. Larger N th root values sharpen the peaks in the vespagram, improving slowness resolvability at small-aperture arrays.

Phase-weighted stacking analysis

In phase-weighted stacking, a coherency measure based on the instantaneous phase provides a weight for each sample of the beam. The instantaneous phase is determined for each array trace using complex trace analysis (Schimmel and Paulsen, 1997). For each array trace $s(t)$, an analytic signal $S(t)$ is constructed with $s(t)$ as the real part and the Hilbert transform $H[s(t)]$ as the imaginary part:

$$S(t) = s(t) + iH[s(t)], \quad (3)$$

which can also be expressed as

$$S(t) = s(t) + iH[s(t)] = A(t) \exp(i\phi(t)). \quad (4)$$

Here, $A(t)$ is the envelope of the trace and $\phi(t)$ is the instantaneous phase (Bracewell, 1965). Schimmel and Paulsen (1997) showed that the sum of two analytic signals $C(\tau) = S_1(\tau) + S_2(\tau)$ is maximal at fixed time $t = \tau$ when the two instantaneous phases are equal. In order to deal with the amplitude variation between the analytic signals, amplitudes are normalized on a sample by sample basis before summation. This leads to the phase stack $c(t)$, obtained independent of the amplitude,

$$c(t) = \frac{1}{M} \sum_{j=1}^M \exp(i\phi_j(t)), \quad (5)$$

where M is the number of traces. The phase stack is a measure of coherency as a function of time that varies between 0 and 1. If two signals have the same phase, $c(t)$ will have a value of 1. In phase-weighted stacking, this coherency value weights the samples of a normal linear stack, such that

$$PWS(t) = \frac{1}{M} \sum s_j(t) c(t)^\gamma. \quad (6)$$

In essence, the phase stack applies a filter that depends on the similarity or dissimilarity of the signals. The sharpness of the filter can be controlled by the power factor γ .

In contrast to the Nth-root stacking process, sliding sub-windows are not used in phase-weighted stacking, because the amplitude is normalized on a sample-by-sample basis prior to coherency weighting. Coherent small-amplitude arrivals consequently have the same weight as coherent large-amplitude arrivals, and thus have the same amplitude in the final vespagram.

Following Nth-root or phase-weighted stacking analysis, we run an arrival detector over the final vespagram image that triggers on peaks over a certain amplitude threshold. The triggered arrival detections can then be compared to predictions from a given velocity model. We have applied both 15th-root and phase-weighted stacking methods to far-regional data recorded on small-aperture arrays in central Asia and show examples of the results in the next section.

Application of Methods to Regional Arrays in Kazakhstan

The Makanchi (MKAR) and Karatau (KKAR) arrays in Kazakhstan record the abundant seismicity that occurs across central and southern Asia. Our current event database is comprised of far-regional distance (14° – 18°) seismograms for earthquakes occurring from 2002 to 2006. In Figure 3 we show the configurations of the arrays as well as database events from 2002–04 recorded at each (or both) of the arrays. The MKAR and KKAR arrays have similar configurations: a central sensor surrounded by 3 sensors in an inner ring, and 5 sensors in an outer ring. The aperture of the outer ring is ~ 2 km at KKAR and ~ 3 km at MKAR. The main instruments at both arrays are vertical-component borehole seismometers (GS-21) recording continuous data at 20 Hz. At KKAR the borehole seismometers are at 50 m depth, and at MKAR they are at 30 m depth. Each array also houses 3-component broadband seismometers; those stations are labeled KK31 and MK31 in Figure 3. In the current study we are only concerned with the vertical channel borehole data.

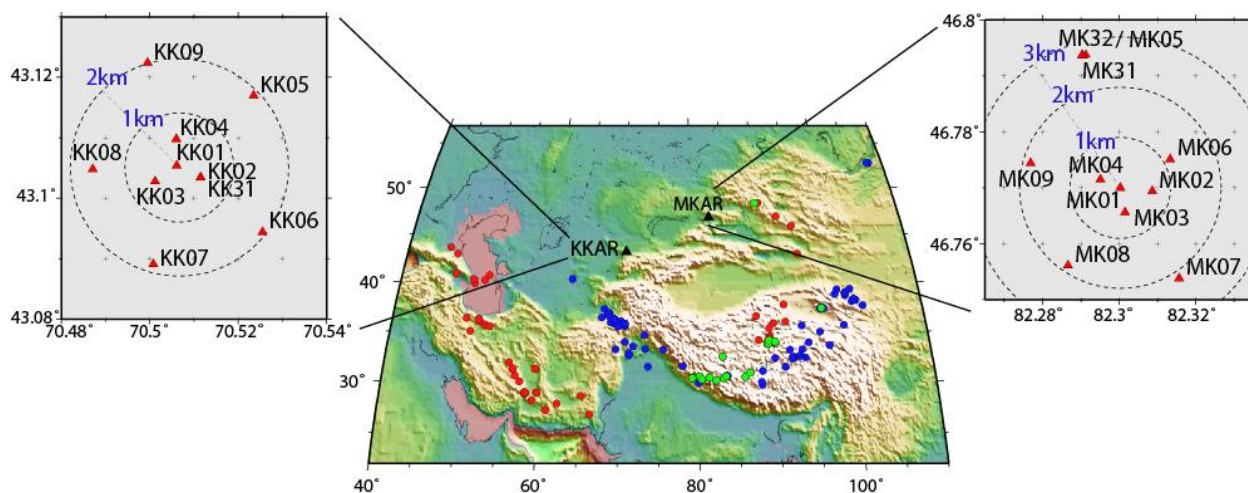


Figure 3. Location map of the KKAR and MKAR arrays and study events. Inset maps show the details of the array configurations. The main map shows the earthquakes (2002–2004) in our study database. Red circles are earthquakes occurring at far-regional distances from KKAR, and blue circles are at far-regional distance from MKAR. Green circles are earthquakes recorded by both arrays at far-regional distances.

To ensure the validity of the hypocenter estimates (particularly the depths), we relocated the events in the database using a grid-search event location algorithm (Rodi, 2006), the AK135 velocity model, and the time-defined phases in the Engdahl, van der Hilst and Buland (EHB) bulletins (Engdahl et al., 1998). We retained those events for which the relocation hypocenters produced small errors in both epicenter and depth. The resulting database contains 72 events observed at KKAR and 97 observed at MKAR. International Seismic Centre (ISC) body-wave magnitudes in our database range from 4.5–6.2 with a mean of 4.9. As shown in Figure 3, most of the events occur southwest to southeast of the arrays, with only a few to the north. This reflects the predominant seismicity patterns in the region, which are associated with interaction between the Indian, Eurasian, and Arabian plates. In general, the arrays have low noise levels, and the earthquakes are well-recorded across the arrays.

Most events in our current database display an emergent first arrival (Figure 4), and we observe few events with obvious impulsive first arrivals, for both KKAR and MKAR events. Since the emergent signal is observed for most events, independent of source location, it's likely that the emergent signal is a consequence of interaction with the upper mantle discontinuity at 410 km, rather than of source effects, such as array orientation along a nodal-plane or a double-couple source mechanism.

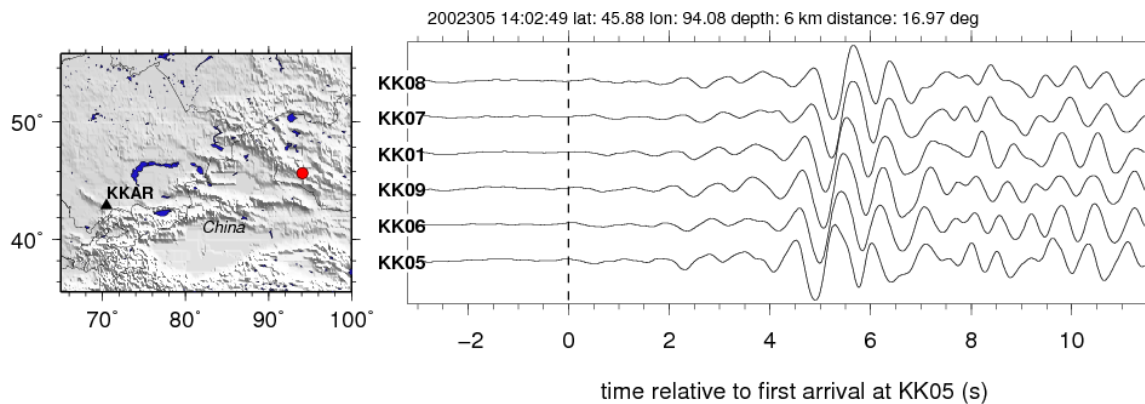


Figure 4. Left: Map showing the event (red circle) and array (triangle) locations. Right: Array gather from the far-regional earthquake recorded at KKAR. Note the emergent first arrivals and the large amplitude energy between 4–7 s. Zero offset corresponds to the first arrival at station KK05.

As we demonstrated earlier with synthetics, the limited aperture of arrays such as MKAR and KKAR creates slowness and arrival-time uncertainties in secondary phase identification. For example, far-regional P waves with horizontal slownesses between 8–11 s/deg traverse a 2–3 km aperture array in 0.2–0.3 s. This very small move-out results in an over-weighting of small slowness values in the beaming process, which causes smearing and reduced resolution in the slowness domain. We have found that eliminating some of the array elements in the secondary phase processing improves slowness and arrival-time estimation. At both KKAR and MKAR, there are four center elements within several 100 m of each other, so we omit those and include only the outer ring of elements and one center element in our stacking procedures.

Another uncertainty in our calculations is in the back azimuth computed for the array-to-event orientation, which is used in our τ - p processing to rotate the array. This back azimuth is computed using assumptions that the event is well-located and that the great-circle path is followed between the event and station (i.e., there is little velocity heterogeneity along the source-to-receiver path). These are significant assumptions, which affect the accuracy and precision of our results if they are incorrect. At far-regional distances a poor event location is less problematic than path heterogeneity in back-azimuth computations. For example, at far-regional distances an event mislocated by as much as 50 km changes the computed back azimuth by less than 0.5° , which has a minimal effect on a slant-stack process. On the other hand, significant path deviations from the assumed great circle can cause problems in the slant-stack computation. For the MKAR and KKAR small-aperture arrays, even a relatively small back-azimuth uncertainty (on the order of 2° – 5°) can change the arrays' distance ordering by ~ 0.6 km for the outer array elements, which is equivalent to a 1–2 sample time shift.

To determine back-azimuth corrections for KKAR and MKAR, we average the back-azimuth residuals observed for our dataset, similar to Mykkeltveit et al. (1990). We use phase-weighted stacking to calculate the coherence values for fixed arrival slowness and varied back azimuth. The maximum coherence above 0.85 is then mapped and the average deviation of the back-azimuth residual is found over the processing window of interest. Figure 5 shows an example of this processing for an event observed at a distance of 14.7° from MKAR. The middle panel of Figure 5 shows the phase-weighted coherence image at all azimuths, and the top panel of Figure 5a shows a zoomed view of the maximum coherence values at each time sample in the processing window, from which the average back-azimuth residual is calculated. The back-azimuth residual for this particular event is -9.2° .

In Figure 6 we show histograms of the percent frequency versus back-azimuth residual for our MKAR and KKAR database. For the complete MKAR dataset we find an average back-azimuth deviation of $-10^\circ \pm 5^\circ$ (observed– predicted) for far-regional arrivals; at KKAR the average back-azimuth deviation is $-4^\circ \pm 8^\circ$. The average back-azimuth residual at both arrays is fairly high, and it is not clear what the source of these large negative residuals is. However, most of the events in our far-regional databases are located in the most heterogeneous lithosphere on Earth. This makes it more likely that lateral heterogeneity along the far-regional path between the earthquake sources and arrays is the primary cause of high back-azimuth residuals, rather than near-receiver structure.

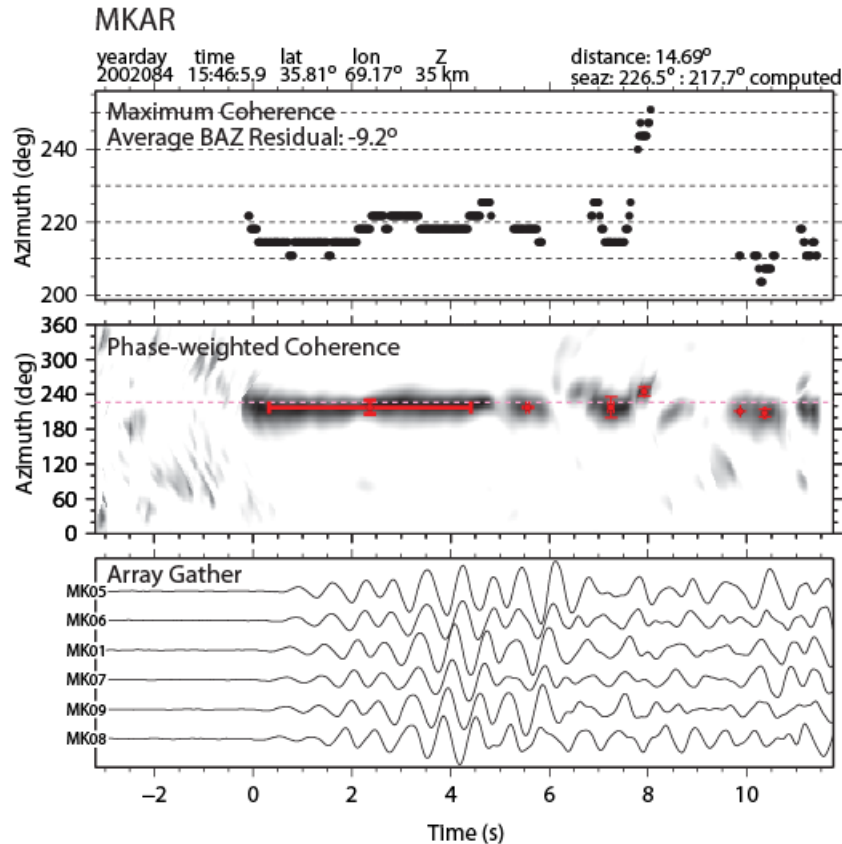


Figure 5. Example of a back-azimuth uncertainty calculation found using phase-weighted stacking. Bottom panel shows the MKAR array waveforms. The middle panels show the results of phase-weighted stacking for the back-azimuth value, and the top panel is a zoom in on the high-value coherence values. This particular example has a back-azimuth residual of -9.2° .

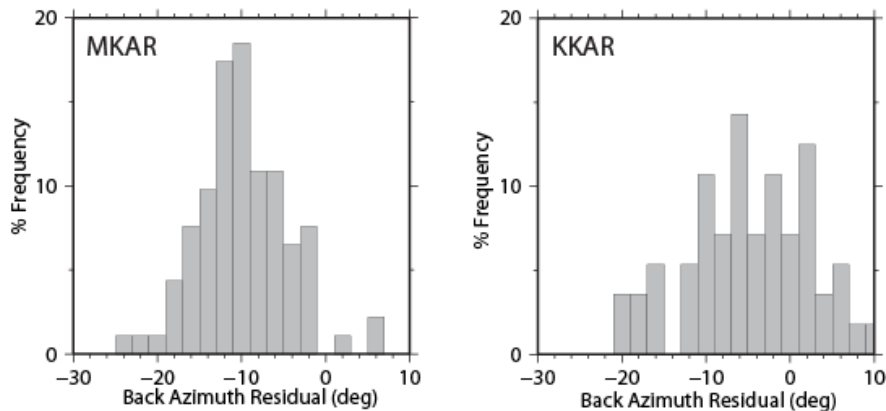


Figure 6. The percent occurrence of particular back-azimuth residuals for the MKAR and KKAR event databases.

Comparison between Nth-Root and Phase-Weighted Stacking

Following the back-azimuth calibration of the MKAR and KKAR arrays, we processed the KKAR and MKAR array data in our event database using 15th-root and phase-weighted stacking methods. As mentioned earlier, we dropped several of the inner array elements in the stacking procedures to further enhance slowness resolution at the small-aperture arrays. For each event, we analyzed a 13-s window of signal, which included the direct P arrival, possible depth phases and arrivals from the 410-km discontinuity. After we applied the two stacking methods, we ran our arrival detection algorithm on the resulting vespa images.

In Figure 7 we illustrate the application of our methods on two events from the database. The left side of Figure 7 shows the analysis of an event in the Himalayas observed at KKAR; the right side of the figure shows the results from an event from the northeastern edge of the Tibetan Plateau observed at MKAR. The top two subpanels in Figure 7 show the best beam computed from the distance-sorted array gather, based on the first-arriving P slowness from the phase-weighted stacking. The bottom two subpanels show the results of applying the 15th-root and phase-weighted stacking analysis to the two event observations. On each of these results we plotted the IASPEI91 predictions for the transition-zone P and pP arrivals (red squares), found using the TauP Toolkit (Crotwell et al., 1999). The IASPEI91 arrival times are relative to the zero-time offset of the closest array element; in other words, we always plot the IASPEI91 first arrival at zero time, regardless of whether it matches the observed first arrival. The presence of more than one red square for a given arrival is an effect of upper-mantle triplication that creates multiple arrivals. We also plotted red crosses at the phase arrivals found by our arrival detection algorithm. The differences between the red crosses and the yellow squares reflect misfit between the reference and actual velocity models along the propagation path, as well as potential differences in the published and actual earthquake depths.

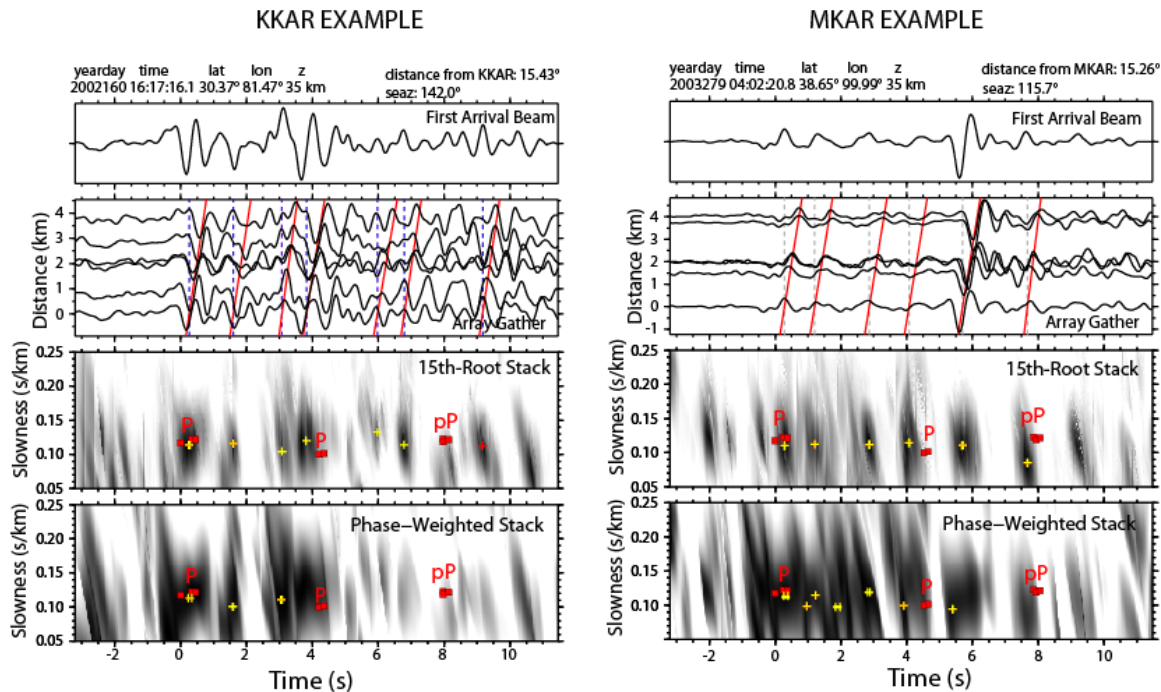


Figure 7. Examples comparing the Nth-root and phase-weighted stacking procedures for far-regional observations at KKAR (left) and MKAR (right). The top two panels show the array best beams and gathers ordered by distance. Red lines are the arrival-time curves based on slowness values computed in the 15th-root results. The bottom two panels are the 15th-root stack and phase-weighted stack vespagrams. Red squares are the IASPEI91-predicted arrival times and slowness; yellow crosses are the arrivals determined from vespa processing.

In general, we find that both methods detect the primary coherent arrivals. In many cases, events with lower levels of noise exhibit sharper arrivals in the 15th-root stacking results. This may be related to the nature of the Nth-root coherency weighting, which appears more effective at suppressing noise. In other words, in the absence of

significant noise, more of the seismogram is weighted similarly, broadening peaks in the vespagram with respect to time. This is evident from a visual comparison between the 15th-root and phase-weighted stacking results of the MKAR example shown in Figure 7.

We also have found that, for the same event, 15th-root and phase-weighted stacking do not always detect the same arrivals. Large amplitude arrivals are almost always detected by both processing methods, but the same does not hold true for weaker arrivals. The differences for weaker arrivals may be caused by the particular implementation of our post-processing arrival detector, which has a tunable threshold that favors larger amplitude arrivals. This is an issue we will continue to address in future work.

Figure 7 also demonstrates that a comparison of the stacking-derived arrival times and slowness to IASPEI91 predictions do not always coincide. The first arrival is usually the best-matched in slowness—within ± 0.02 s/km. Subsequent arrivals are more difficult to pair up by arrival time, but generally have slowness values within ± 0.04 s/km of nearby predicted arrivals, albeit with significant scatter.

CONCLUSIONS AND RECOMMENDATIONS

The small aperture (~2–3 km) of many of the recent regional arrays installed for nuclear monitoring purposes restricts their usefulness at far-regional distances, where triplicated arrivals from the upper-mantle discontinuities make phase identification more difficult. Our research is focused on developing methods to accurately determine the slowness and arrival time of primary and secondary arrivals at these distances, with the final goal of incorporating the results in computations for event location and magnitude determination. We have found that we can adapt familiar array-processing techniques to the far-regional phase detection problem. Specifically, we are successfully applying 15th-root and phase-weighted stacking to emphasize small, coherent arrivals that occur in a 15–25 s window following the initial P-wave arrival. The processing adaptations that we have employed reduce the strong smearing effects that occur in slowness space at small-aperture arrays.

We have applied our techniques to a large database of moderate-sized earthquakes occurring at far-regional distances from two arrays in central Asia. Our results indicate that we can differentiate between closely spaced arrivals in the early body-wave coda. However, it is also apparent that in many cases a simple global reference model cannot capture the phase succession and arrival-time behavior in the complex tectonic regions of central and southern Asia. In our continuing work under this project we will focus on developing “templates” of typical events and associated phase behavior. These templates will be supported by accurate 1-D velocity models and full-waveform modeling, in specific regions such as Iran, Turkmenistan, Pakistan, northern India, and western China.

REFERENCES

- Bracewell, R. N. (1965). *The Fourier transform and its applications*. New York: McGraw-Hill.
- Crotwell, H. P., T. J. Owens, and J. Ritsema (1999). The TauP Toolkit: Flexible seismic travel-time and ray path utilities, *Seism. Res. Ltrs.* 70: 154–160.
- Engdahl, E. R., R. van der Hilst and R. Buland (1998). Global teleseismic earthquake relocation with improved travel times and procedures for depth determination, *Bull. Seis. Soc. Am.* 88: 722–743.
- Kennett, B. L. N. and E. R. Engdahl (1991). Travel times for global earthquake location and phase identification, *Geophys. J. Int.* 105: 429–465.
- Kennett, B. L. N., E. R. Engdahl, and R. P. Buland (1995). Constraints on seismic velocities in the earth from traveltimes, *Geophys. J. Int.* 122: 108–124.
- Muirhead, K. J. and R. Datt (1976). The Nth root process applied to seismic array data, *Geophys. J. R. Astron. Soc.* 47: 197–210.
- Mykkeltveit, S., F. Ringdal, T. Kvaerna, and R. W. Alewine (1990). Application of regional arrays in seismic verification research, *Bull. Seis. Soc. Am.* 80: 1777–1800.
- Rodi, W. (2006). Grid-search event location with non-Gaussian errors, *Phys. Earth & Planet. Int.* 158: 55–66.

29th Monitoring Research Review: Ground-Based Nuclear Explosion Monitoring Technologies

Rost, S. and C. Thomas (2002). Array seismology: methods and applications, *Rev. Geophys.* 40: 1008, doi:10.1029/2000RG000100.

Schimmel, N. and H. Paulssen (1997). Noise reduction and detection of weak, coherent signals through phase weighted stacking, *Geophys. J. Int.* 130: 497–505.